

DMI Report 17-17

Radar backscatter modelling for sea ice radar altimetry

**Improve the understanding of the influence of snow properties
on radar return
(The ESA sea ice climate change initiative phase 2 WP2220)**



Colophon

Serial title

DMI Report

Title

Radar backscatter modelling for sea ice radar altimetry

Subtitle

Improve the understanding of the influence of snow properties on radar return (The ESA sea ice climate change initiative phase 2 WP2220)

Author

Rasmus T. Tonboe

Other contributors

Responsible institution

Danish Meteorological Institute

Language

English

Keywords

Sea ice, radar altimetry, sea ice thickness

Uri

www.dmi.dk/dmi/sr

Digital ISBN

978-87-7478-671-9

ISSN**Version**

19 April 2017

Website

www.dmi.dk

Copyright

DMI

Content

| | |
|-------------------------------------|----|
| Abstract..... | 5 |
| Resumé..... | 5 |
| 1. Introduction..... | 6 |
| 2. Snow and ice data | 8 |
| 3. Model description..... | 8 |
| 4. Simulation results | 10 |
| 5. Discussion and conclusions | 15 |
| References..... | 17 |
| Previous reports | 19 |

Abstract

Although it is well known that radar waves penetrate into snow and sea ice, the exact mechanisms for radar-altimeter scattering and its link to the depth of the effective scattering surface from sea ice are not well known experimentally. Previously proposed mechanisms linked the snow ice interface, i.e. the dominating scattering horizon, directly with the depth of the effective scattering surface. However, simulations using a multilayer radar scattering model show that the effective scattering surface is affected by snow-cover and ice properties. In this study we evaluate the effective scattering surface in terms of floe buoyancy and radar penetration using both a scattering model and “Archimedes’ principle” and data from the project round robin data base. A relationship between the effective scattering surface depth and the snow cover was found. However, this requires empirical evidence to confirm for natural snow packs. This report was made as part of ESA’s sea ice climate change initiative project.

Resumé

Selv om vi ved at radar mikrobølger trænger ind i sne og havis kender vi ikke detaljerne ved radar altimeter mikrobølge spredning og sammenhængen til dybden af spredningsoverfladen eksperimentelt. Tidligere har det været foreslået at sne-is overgangen som er den dominerende spredningsoverflade er sammenfaldende med med den effektive spredningsdybde. Dog viser simuleringer med en mange-lags radar spredningsmodel at den effektive spredningsdybde bliver påvirket af sneen og isoverfladen. I dette simulerings eksperiment undersøger vi den effektive spredningsdybde og isens isostatiske ligevægt ved hjælp af en mange-lags spredningsmodel, Arkimedes lov og data fra målinger. Ud fra simuleringerne har vi fundet en sammenhæng imellem den effektive spredningsdybde og snedækket. Denne sammenhæng bør efterprøves med målinger fra naturlige sneforhold på havis. Denne rapport er skrevet som en del af ESA’s *sea ice climate change initiative* projekt.

1. Introduction

Variation in sea ice thickness is a significant indicator for climate change (Wadhams, 1990; Rothrock et al., 2003), but its inter-annual, seasonal and spatial variability is poorly resolved (McLaren et al., 1992). Therefore, much interest is being paid to alternative methods for monitoring sea ice thickness for climate monitoring such as satellite radar altimetry (Laxon et al., 2003; Wingham, 1999; Wingham et al., 2006), and laser altimetry using ICESAT 1 (Kwok et al., 2006; Kwok and Cunningham, 2008; Farrell et al., 2009). The ice thickness is derived from altimeters by multiplying the measured freeboard height by an effective snow/ice density factor and adding an offset. For example, Alexandrov et al. (2010) gives the following equation for the ice thickness H_i as a function of the ice freeboard F_i using Sever data (see section 2):

$$H_i = 8.13F_i + 0.37 \quad (1)$$

It is commonly assumed that radar altimeter signals operating at an electromagnetic frequency of about 13 GHz penetrate to the snow/ice interface or ice freeboard, F_i , also the free variable given in Eq. 1. However, for pulse limited space-borne radar altimetry, modelling indicates that snow depth and density as well as snow and sea ice surface roughness influence the radar penetration into the snow and ice even for cold homogeneous snow packs in winter (Tonboe et al., 2010). As a result, the effective scattering surface depth, which is the horizon where the freeboard is measured, can vary as a function of these snow and ice properties (Tonboe et al., 2006a). In addition, snow depth and density and ice density critically affect the floe buoyancy and the chances for estimating sea ice thickness by measuring its freeboard (Rothrock, 1986; Giles et al., 2007; Alexandrov et al., 2010). The freeboard height is multiplied by the effective density to estimate the ice thickness for a floe in hydrostatic equilibrium. Actually, the ice floe may not be in hydrostatic equilibrium on a point-by-point basis (Doronin and Kheisin, 1977), and this turns out to have consequences for the height measurements using a radar altimeter (Tonboe et al., 2010). Some surface types often related to ice type or thickness category (first-year ice, refrozen melt-ponds) have much higher (10 times) backscatter than other surface types (multiyear ice hummocks, deformed ice) and this affects the effective scattering surface detected by the track-point.

Several ice thickness point measurements are needed to characterise the ice thickness distribution representative of a particular ice-covered region (Rothrock, 1986; Haas, 2003). The mode of the ice thickness distribution represents the dominating thermodynamically grown thickness of level ice. However, the distribution has a tail towards thicker ice, i.e. deformed ice, and the average may be significantly different from the mode (Haas, 2003). Typical ice thickness distributions from the Fram Strait and the Lincoln Sea are shown in Fig. 1.

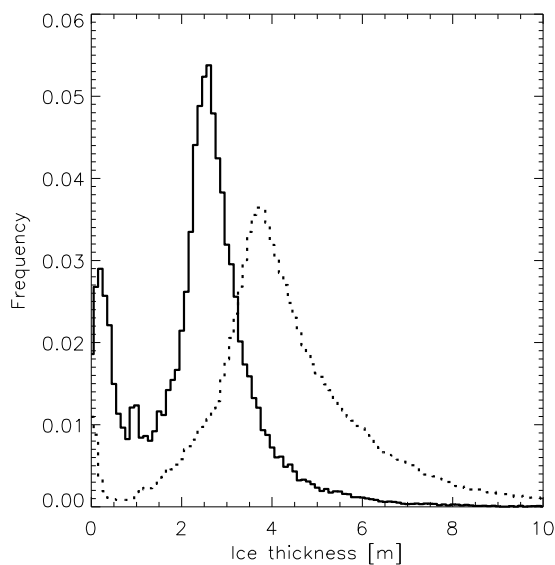


Figure 1. Typical ice thickness distributions measured with a helicopter-borne electromagnetic induction device: Fram Strait, 13 April 2003 (full-line) and Lincoln Sea, 12 May 2004 (dashed line).

As the ice freeboard has to be multiplied by about 10 to obtain the thickness, even small errors in the freeboard retrieval lead to large ice thickness estimation errors (Rothrock, 1986). This multiplication factor derived from the effective density is not constant and may vary between different thickness categories, i.e. new-ice and multiyear ice, as well as seasonally and regionally (Haas et al., 2006a, Wadhams et al., 1992). This is why auxiliary data such as snow thickness, snow density, ice density are used in the processing of altimeter data for deriving the ice thickness (Ricker et al., 2016). Tonboe et al. (2006b) pointed out that the parameters affecting the sea ice freeboard and the radar penetration and ice type distribution are not always mapped during field campaigns. The error-bars on the retrieved ice thickness estimates are needed when the data are assimilated into numerical models or when they are compared to other ice thickness estimates such as those from laser altimeters, submarine sonar, drilling, snow radars and electromagnetic induction instruments (Kern et al., 2015). It is further important to identify the largest and most important error sources so that these can be assessed during field campaigns and using remote sensing. Rothrock (1986) stated that the uncertainties involved in deriving the ice thickness from its freeboard were too large. However with the advent of modern space borne altimeters the issue has been revisited. Error estimates of the ice thickness retrieval uncertainty for both laser (total error 0.76 m) and radar (total error 0.46 m) altimeters by Giles et al. (2007) included errors sources related to the floe buoyancy: i.e. the snow depth, freeboard estimation uncertainty, and the snow, ice and water density. The snow depth estimation error resulting in an ice thickness estimation error of 0.1 m in Giles et al. (2007) for the radar altimeter was the most important of the error sources. The error due to radar penetration was assumed negligible in their budget, and the error due to systematic height and radar backscatter variability within the footprint was not considered (Tonboe et al. 2010).

The specific aim of this study is to evaluate the radar altimeter sea ice effective scattering surface in terms of both floe buoyancy and radar surface penetration combining a radar scattering model with “Archimedes’ principle” (Archimedes, 287-212 BC).

2. Snow and ice data

This study is using data which are included in the round robin data package. In particular the data with the most complete description of the snow cover density and thickness.

In situ data of snow and ice properties in the Central Arctic have always been sparse, but to overcome this problem there has been a long history of expeditions. From 1937 to 1991, the Soviet Union operated the series of North Pole drifting stations on multi-year ice floes (Frolov et al., 2006). Some of the data from the North Pole drifting stations have been included in the round robin data package and collocated with altimeter data. In addition to the year round drifting stations the Sever Project collected snow and ice data at on-ice aircraft landing sites from 1928 to 1989. The Sever data were collected primarily during spring and not during summer melt, i.e. at the end of winter and therefore representing maximum thickness. The measurements were distributed geographically across the Arctic Ocean, but with higher frequency in the Eastern Arctic. The National Snow and Ice Data Center (NSIDC) received a subset of the Sever data also including data from the drifting stations (NSIDC, 2004). The data are described in Warren et al. (1999) (hereafter W99) and they are also included in the round robin data package.

In order to bridge the gap in time between the satellites ICESAT 1 and 2 laser altimeter missions and calibrate ICESAT 2 NASA is operating an aircraft campaign programme called operation ice bridge (OIB). ICESAT 1 operated from 2003 to 2010 and ICESAT 2 will be launched in 2017. On board the aircraft which is flown in polar regions there are several scientific instruments including a scanning laser altimeter and a snow radar.

The “ESACCI-SEAICE-RRDP2-SIT-OIB-IDCSI4_ARCTIC.dat” file in the round robin data package is a collection of the operation ice bridge data, W99 climatology, Cryosat2 and ENVISAT freeboard data and the numerical ice/ocean model NEMO snow depth data. The file has the following data fields:

Observation ID, time-date, latitude, longitude, CryoSat2 AWI freeboard, CryoSat2 ESA freeboard, ENVISAT freeboard, ENVISAT freeboard, OIB laser freeboard, OIB snow depth, OIB surface roughness, W99 snow depth, W99 density, NEMO snow depth.

3. Model description

The radar scattering model is a multilayer one-dimensional radiative transfer model where surface scattering is computed at horizontal interfaces (snow surface, icy layers and ice surface), as described in Tonboe et al. (2006a) and Tonboe et al.(2010). Propagation speed, attenuation and scattering are computed for each layer. The simulated echo delay due to freeboard variations and the time dependent backscatter intensity which is recorded onboard the satellite are integrated afterwards in a waveform model suitable for pulse limited space borne altimeters to compute the track point. The track point is a point in time mid between the onboard satellite received backscatter noise floor and the maximum signal power. The track point is computed at 0.35, 0.50, 0.65, and 0.80 of the maximum signal power. The effective scattering surface is the level detected by the track point. On ice sheets, in regions where surface scattering dominates, the $\frac{1}{2}$ - power time re-tracking threshold gives a good representation of the mean surface elevation (Davis, 1997). It is a robust measure of the distance to the effective scattering surface: simulations using seasonal output from a thermodynamic model (snow cover parameters but not surface roughness or ice parameters) as input to the backscatter model show that the scattering surface follows the

ice surface within about 5 cm during winter (Tonboe et al., 2006b). The model concept is different from single layer scattering models developed for ice sheet backscatter (e.g., Ridley and Partington, 1988) since surface scattering dominates in sea ice i.e. scattering from the snow and ice surfaces and possibly from layers within the snow.

The forward model uses a set of snow and ice microphysical parameters for each layer: temperature, layer thickness, density, correlation length (a measure of the snow grain size or the ice inclusion size), interface roughness, salinity, and snow wetness to compute the effective scattering surface. The permittivity of dry snow is primarily a function of snow density, and the permittivity of sea ice is primarily a function of salinity and temperature. The permittivity of both materials is computed using the mixing formulae for ice spheres (Mätzler, 1998):

$$\varepsilon_{eff} = \frac{2\varepsilon_1 - \varepsilon_2 + 2v(\varepsilon_2 - \varepsilon_1) + \sqrt{(2\varepsilon_1 - \varepsilon_2 + 3v(\varepsilon_2 - \varepsilon_1))^2 + 8\varepsilon_1\varepsilon_2}}{4}, \quad (2)$$

where v is the fraction of volume occupied by inclusions, ε_1 is the host permittivity of the material surrounding the inclusions and ε_2 is the permittivity of the inclusions. For snow ε_1 is the permittivity of air ($\varepsilon_{air}=1$), and for saline ice, ε_1 is the permittivity of pure ice given in Mätzler et al. (2006). For snow the inclusions are pure ice, and the background is air. For saline first-year ice the inclusions are brine pockets and the background is pure ice. The permittivity and also the volume of brine are given in Ulaby et al. (1986). For multiyear ice the host material is saline ice (the same as for first-year ice) and the inclusions are air bubbles. The inclusions also act as scatters of the microwave radiation. For the altimeter the volume scattering is important for the extinction of the signal but it is insignificant as a backscatter source. The backscatter is dominated by surface scattering mechanisms and scattering in the ice does therefore not affect the simulations.

Surface scattering is the scattering at dielectric interfaces such as the air-snow and snow-ice interface. The nadir-looking surface backscatter is a function of the nadir reflection coefficient $|R(0)|$ and the flat-patch area F (Fetterer et al., 1992), i.e.

$$\sigma^{surf} = 0.9F|R(0)|^2 \frac{H}{u\tau}, \quad (3)$$

where H is the satellite height, u the pulse propagation speed (speed of light in air, snow and ice respectively) and τ the pulse length. F is the fraction of the flat-patch area, which is inversely related to roughness (i.e., smooth surfaces have high F). F is unitless. This model assumes that the signal is dominated by reflection processes from relatively small plane areas (flat-patches) normal to the incident signal within the footprint. In the review of different surface scattering models in Fetterer et al. (1992) the approach in Eq. 3 is believed to be “more realistic” than other models. The geometrical optics model, which is an alternative to Eq. 3, makes very similar predictions. The basic concept for all altimeter surface scattering models is that the backscatter is a function of reflection coefficient and surface roughness; i.e., when the surface is smooth the backscatter is high, and when the surface is rough then the backscatter is smaller. All models described in Fetterer et al. (1992), including Eq. 3, make that prediction.

The improved Born approximation, suitable for microwave scattering in a dense medium such as snow, is used to compute the volume scattering coefficient (Mätzler, 1998; Mätzler and Wiesmann, 1999). Volume scattering is scattering from particles or inclusions within layers, i.e. snow grains within the snow layers, and air bubbles and brine pockets within the ice layers.

The improved Born approximation for spherical inclusions is (Mätzler, 1998)

$$\sigma^{vol} \cong \frac{3p_{ec}^3 k^4}{32} v(1-v) \left| \frac{(\varepsilon_2 - \varepsilon_1)(2\varepsilon_{eff} + \varepsilon_1)}{2\varepsilon_{eff} + \varepsilon_2} \right|^2, \quad (4)$$

where p_{ec} is the correlation length, k the wavenumber, v the volume fraction of scatters, and ε_1 , ε_2 , ε_{eff} are the permittivity of the background, the scatters, and the layer, respectively. Volume scattering is an important backscatter mechanism for scatterometers operating at 13GHz and about 50° incidence such as QuikScat SeaWinds. However, the total altimeter backscatter is dominated by surface (or interface) scattering, and in our altimeter simulations volume scattering is insignificant as a backscatter source. This is in agreement with laboratory experiments showing that at nadir incidence, volume scattering is insignificant as a backscatter source for snow-covered sea ice (Beaven et al., 1995). Though volume scattering is not a backscatter source, it does increase extinction and to some extent the distribution of backscatter between the snow and the ice surface. This distribution and the snow depth do affect the depth of the effective scattering surface (Tonboe et al., 2006a, Tonboe et al., 2010).

No specific correction is applied for antenna gain or pulse modulation in the characterisation of the emitted pulse. We use a geometric description of the footprint area in each layer i as a function of time t from Chelton et al. (2001) for a pulse-limited altimeter,

$$A_i(t) = \frac{\pi u_i t H}{1 + H/R_e} - \frac{\pi u_i (t - \tau) H}{1 + H/R_e}, \quad (5)$$

where the second term is 0 when $t < \tau$. R_e is Earth's radius (6371 km), u_i is the speed of light in the layer and H is the satellite height (730 km).

The waveform model integrates the time-dependent backscatter from each scattering horizon. The pulse propagation speed, signal extinction and backscatter are computed as the pulse penetrates the profile, and each individual contribution is summed with appropriate time delay. The backscattered energy, E , measured at the satellite for each model time-step (1×10^{-11} s or approximately 3 mm in free space), is the sum of the footprint area, A_i , multiplied by the layer backscatter coefficient, σ_i , i.e.

$$E_t = \sum_{i=1}^n A_i \sigma_i. \quad (6)$$

The layer backscatter coefficient includes volume backscattering though its magnitude is negligible. The backscatter coefficient from each layer is adjusted for extinction using the radiative transfer approach, i.e.

$$\sigma_{total} = (\sigma_i^{surf} + T_i^2 \sigma_i^{vol}) \prod_{i=1}^n \frac{1}{L_{i-1}} T_{i-1}^2. \quad (7)$$

L is the loss and T the transmission coefficient where $L_0 = T_0 = 1$ for the first layer and σ^{vol} is the negligible volume backscatter coefficient. The waveform model is using a 10^{-11} s time-step.

4. Simulation results

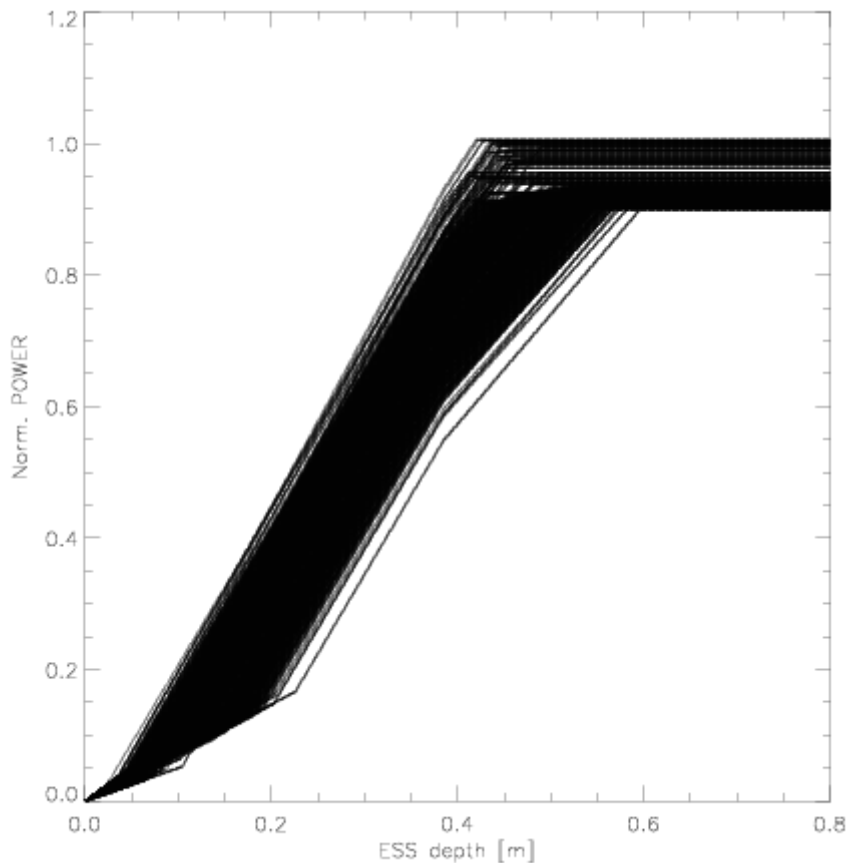
A reference profile in table 1 is used together with measured distributions of snow depth and snow density as input to the model to simulate the radar penetration variability of homogeneous un-layered snow packs during winter. Since both the height of the scattering surface and the floe buoyancy are affected by snow depth and snow density, the scattering model is used together with

“Archimedes’ principle” to compute the sensitivity of both simultaneously. The surface roughness affects the height of the scattering surface and the ice density affects primarily the floe buoyancy. Snow measurements are input to the model in order to translate the natural snow variability to simulated range variability. The scattering model is thus initiated with the snow and ice profile described in Table 1. For each simulation the snow density and the snow depth in Table 1 are exchanged by the OIB snow depth and the W99 snow density from the round robin data file (see Section 2). This produces from the model a backscatter coefficient, penetration depth, waveform, and effective scattering surfaces for track points at 0.35, 0.5, 0.65, 0.80 of the maximum power.

| Layer Number | T [K] | Roughness F | Density [kg/m ³] | Depth [m] | Corr. length [mm] | Salinity [ppt] | Type |
|--------------|--------|-------------|------------------------------|------------|-------------------|----------------|------|
| 1 | 263.15 | 0.01 | 300 | 0.2 | 0.1 | 0.0 | Snow |
| 2 | 268.15 | 0.01 | 900 | 3.5 | 0.2 | 3.0 | Ice |

Table 1. Input to the altimeter model. T is the temperature of the layer, Roughness is quantified as the flat-patch-area the fraction of specular facets compared to the total area (F) described in eq. 3, Density is the density, Depth is the layer thickness, correlation length is a measure of the scatter size (and distribution), Salinity of the layer. Variable marked with **bold** are exchanged with values from the round robin dataset for each simulation.

All simulated leading edge wave forms are shown in Figure 2. The effective scattering surface depth is measured from the snow surface. The one-way travelling time is multiplied with the speed of light (in free space) to scale it to a range measurement following Ricker et al. (2014).



Figur 2. The simulated effective scattering surface (ESS) depth [m] (delay times the speed of light) vs. the normalized power using the operation ice bridge data file as input to the model.

The simulated freeboard using a constant ice thickness of 3.5 m and ice density of 900 kg/m^3 , the OIB snow thickness and the Warren et al., (1999) climatology snow density is shown together with the measured freeboard from Cryosat2 using the AWI processor. There is some coincidence between the highs and lows especially between data points 200 and 800. A perfect match is not expected considering the many unknown parameters in the simulation (surface roughness, ice density, ice thickness, snow-pack vertical structure and sub-foot-print spatial variability of all these above parameters). However, it shows that the OIB snow depth data are useful on this spatial (25-50km) scale for computing the buoyancy of the floe.

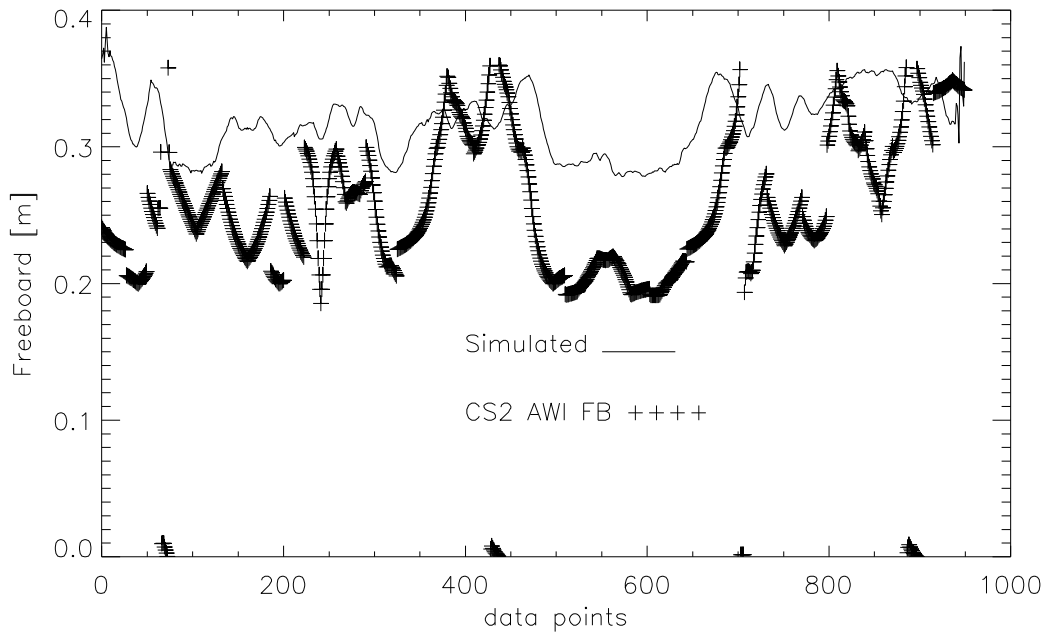


Figure 3. The simulated freeboard using the track point at 0.5 of the peak power (half-power) and the Cryosat2 measured freeboard using the AWI processor. A 20 point uniform low pass filter has been applied to the simulated data.

In the round robin data file the OIB snow depth and the W99 snow density are not correlated and even though the data points in Figure 4 are shown together they are not necessarily connected in time and space. Each of the simulated points is therefore independent.

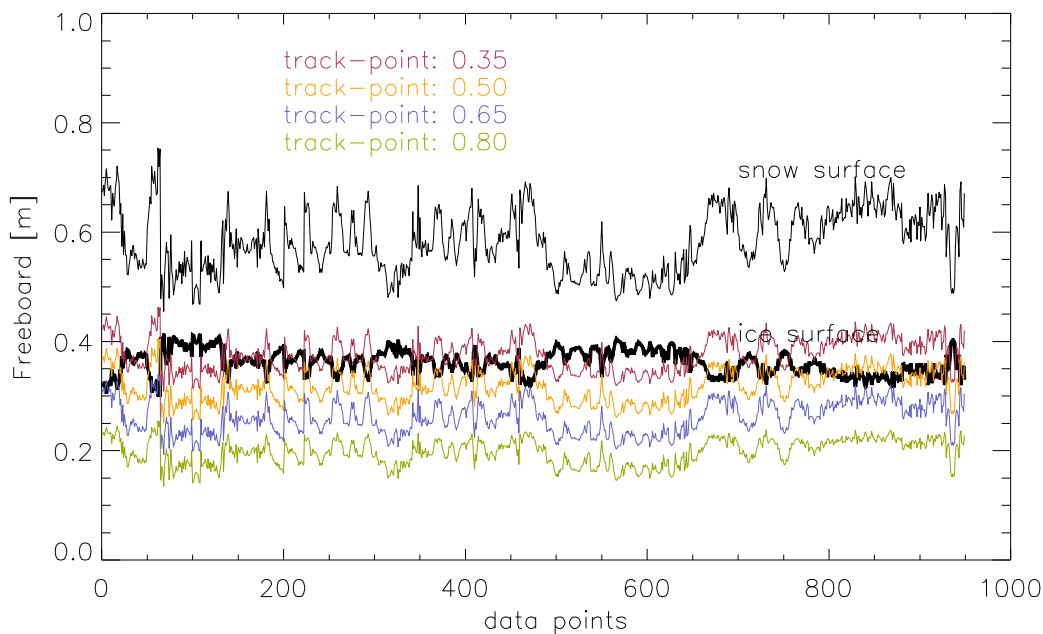


Figure 4. The snow surface, the ice surface and the effective scattering surface for 4 different track-points. The thin black is the snow surface, the bold black is the snow ice interface and the red, orange, blue and green are the effective scattering surfaces for different track-points.

The match-up between the effective scattering surface using the different track points and the ice freeboard is quantified in Table 2. The mean is the mean difference between the ice freeboard and the effective scattering surfaces. Because the slope of the leading edge between all of the track points is nearly the same the spacing between the effective scattering surfaces using the different track points is also the same, about 0.05-0.06 m. The STDDEV of the difference between the ice freeboard and the effective scattering surfaces is given in the last row of Table 2. It shows that it is not important where to set the track point to minimize sensitivity to snow depth and snow density. This is true for this dataset with a very narrow distribution of snow depths. However, other simulations (not shown) with deeper snow up to 1 m show a decrease in the STDDEV with higher track points from 0.35 to 0.8.

| Track-point | 0.35 | 0.50 | 0.65 | 0.80 |
|-------------|---------|--------|--------|--------|
| Mean [m] | -0.0138 | 0.0459 | 0.102 | 0.164 |
| STDDEV [m] | 0.0513 | 0.0513 | 0.0512 | 0.0452 |

Table 2. comparing the ice freeboard with the effective scattering surface at different track-points (fraction of the maximum power) using the OIB dataset and the profile in Table 1.

Figure 5 is almost the same as Fig. 4 except that in this simulation the snow surface has been made smoother (F is 0.02 instead of 0.01). This raises the effective scattering surfaces by about 0.02 m (table 3). Exactly the same result would have been achieved by making the ice surface rougher (set F to 0.005 instead of 0.01 when the snow surface F is 0.01)

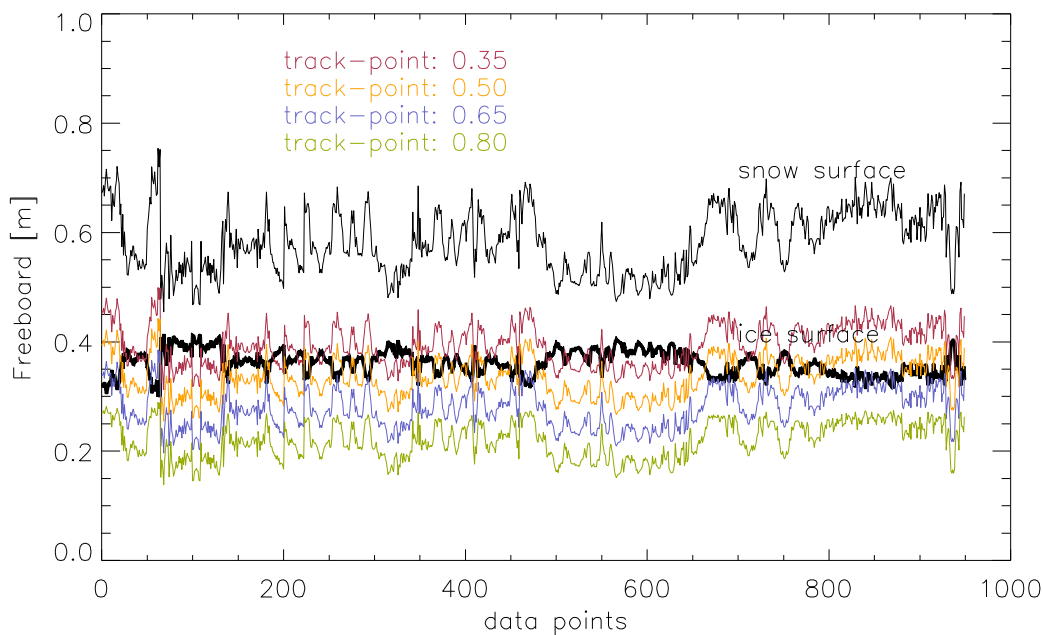


Figure 5. The same as in figure 2 but with a smoother snow surface (F: 0.02).

| Track-point | 0.35 | 0.50 | 0.65 | 0.80 |
|-------------|---------|--------|--------|--------|
| Mean [m] | -0.0322 | 0.0254 | 0.0831 | 0.142 |
| STDDEV [m] | 0.0578 | 0.0578 | 0.0578 | 0.0552 |

Table 3. comparing the ice freeboard with the effective scattering surface at different track-points (fraction of the maximum power) using the OIB dataset and the profile in table 1 except that the snow surface roughness is set to 0.02 (smoother snow surface).

The snow depth and the snow density affect the effective scattering surface and the buoyancy of the floe in opposite directions (Tonboe et al., 2010). However, in the OIB round robin dataset the snow depth and the density are not correlated ($r=-0.25$) and each of the simulations are using independent input. In this dataset the variability of the snow depth is much larger than the variability of the snow density. At least the snow depth variability dominates the way the simulated effective scattering surface is affected. In Figure 6 the snow depth and the snow density is combined (by multiplication) in the snow water equivalent (SWE). The simulated effective scattering surface and ice freeboard difference is directly proportional to the SWE (Fig. 6). Actually because the snow depth variability dominates this simulation the linear relationship to the effective scattering surface and ice freeboard difference is due to snow depth and not density. Roughly, for every millimeter SWE the effective scattering surface is raised by 2 mm relative to the ice freeboard.

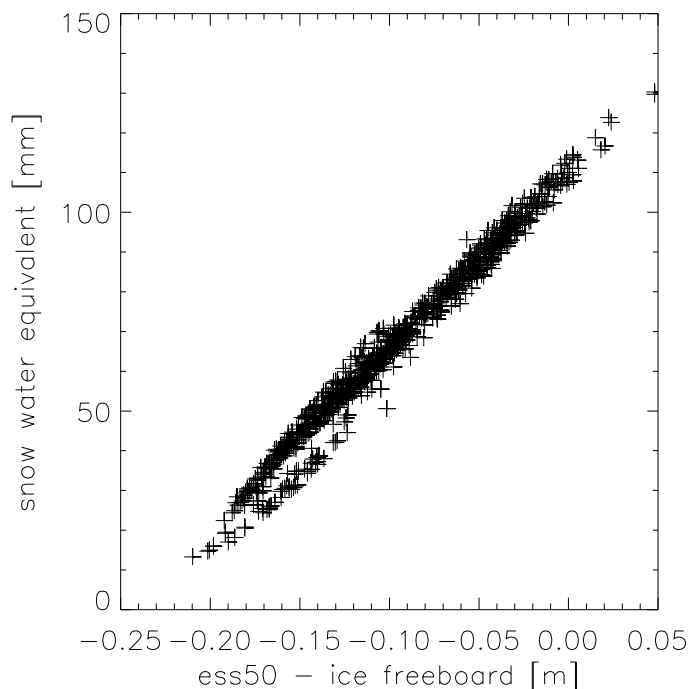


Figure 6. The effective scattering surface (ess) with the track-point at 0.5 x peak-power vs the snow water equivalent (multiplication of the density and snow depth and given in millimeter water).

5. Discussion and conclusions

It is important to identify the most significant error sources so that these can be monitored and the ice thickness estimates corrected accordingly. Even though there are some differences in recent estimates of the variability of the snow and ice parameters affecting the floe buoyancy and the ice thickness retrieval uncertainty estimates, it is clear that four parameters are important: snow depth, ice density, freeboard estimation error and snow density. The simulations in this study show that the radar penetration variability is as important an error source as those affecting the floe buoyancy.

Internal structure and layering is an inherent part of natural snow packs. Icy crusts and layers are formed in the snow due to wind-packing and temporary melt events. The on-going metamorphosis of the snow pack makes the snow grains grow in size and the snow pack is gradually compacted. That kind of detail is not available on satellite footprint scale and so these processes have been ignored in this simulation study. A structured snow pack would raise the effective scattering surface compared to an unstructured snow pack which is used in the simulations. Therefore the simulations represent a lower level for the effective scattering surface.

A relationship between the effective scattering surface depth and the SWE was found based on the simulations with input from the round robin OIB data file. Empirical evidence is required to confirm and possibly quantify this relationship on natural snow packs. Unfortunately this was not possible given the information in the round robin data package.

References

- Alexandrov, V., S. Sandven, J. Wahlin, O. M. Johannesen. The relation between ice thickness and freeboard in the Arctic. *The Cryosphere* 4, 373-380, 2010.
- Archimedes. 1897. On floating bodies I. in T. L. Heath. *The works of Archimedes*. Dover publications, Inc., New York.
- Beaven, S. G., Lockhart, G. L., Gogineni, S. P., Hosseinmostafa, A. R., Jezek, K., Gow, A. J., Perovich, D. K., Fung, A. K., and Tjuatja, S. 1995. Laboratory measurements of radar backscatter from bare and snow-covered saline ice sheets, *International Journal of Remote Sensing*, Vol. 16, No. 5, pp. 851-876.
- Chelton, D. B., J. C. Ries, B. J. Haines, L.-L. Fu, P. S. Callahan. Satellite altimetry. pages 1-131. In: L.-L. Fu & A. Cazenave (Eds.) "Satellite Altimetry and Earth sciences". Academic press 2001.
- Davis, C. 1997. A robust threshold retracking algorithm for measuring ice sheet surface elevation change from satellite radar altimeters. *IEEE Transactions on Geoscience and Remote Sensing*, Vol. 35, No. 4, pp. 974-979.
- Dierking, W., Carlström, A., Ulander, L. M. H. 1997. The effect of inhomogeneous roughness on radar backscattering from slightly deformed sea ice. *IEEE Transactions on Geoscience and Remote Sensing*, Vol. 35, No. 1, pp. 147-159
- Doronin, Y. P., and Kheisin, D. E. 1977. *Sea ice*. Amerind Publ. Co. Pvt. Ltd., New Delhi.
- Farrell, S. L., Laxon, S. W., McAdoo, D. C., Yi, D., and Zwally, H. J. 2009. Five years of Arctic sea ice freeboard measurements from the Ice, Cloud and land Elevation Satellite, *Journal of Geophysical Research*, Vol. 114, C04008, doi:10.1029/2008JC005074.
- Fetterer, F. M., Drinkwater, M. R., Jezek, K. C., Laxon, S. W. C., Onstott, R. G., and Ulander, L. M. H. 1992. Sea ice altimetry. In: *Microwave Remote Sensing of Sea Ice*, Geophysical Monograph 68, edited by: Carsey, F. D., Washington DC, pp. 111-135, American Geophysical Union.
- Frolov, I. E., Gudkovich, Z. M., Radionov, V. F., Shirochkov, A. V., and Timokhov, L. A. 2006. *The Arctic Basin - Results from the Russian Drifting Stations*, Springer Praxis Books.
- Giles, K. A., Laxon, S. W., and Raney, R. K. 2007. Combined airborne laser and radar altimeter measurements over the Fram Strait in May 2002. *Remote Sensing of Environment*, Vol. 111, pp. 182-194.
- Haas, C. 2003. Dynamics versus thermodynamics: the sea ice thickness distribution, in: *Sea ice*, edited by: Thomas, D. N. and Dieckmann, G. S., Blackwell.
- Haas, C., Goebell, S., Hendricks, S., Martin, T., Pfaffling, A., and von Saldern, C. 2006a. Airborne electromagnetic measurements of sea ice thickness: Methods and applications. *Arctic Sea Ice Thickness: Past, Present and Future*, edited by: Wadhams and Amanatidis, *Climate Change and Natural Hazards Series 10*, EUR 22416.
- Kern, S., K. Khvorostovsky, H. Skourup, E. Rinne, Z. S. Parsakhoo, V. Djepa, P. Wadhams, S. Sandven. The impact of snow depth, snow density, and ice density on sea ice thickness retrieval from satellite radar altimetry: results from the ESA-CCI sea ice ECV project round robin exercise. *The Cryosphere* 9, 37-52, 2015.
- Kwok, R. and Cunningham, G. F. 2008. ICESat over Arctic sea ice: Estimation of snow depth and ice thickness. *Journal of Geophysical Research*, Vol. 113, C08010, doi:10.1029/2008JC004753.
- Kwok, R., Cunningham, G. F., Zwally, H. J., and Yi, D. 2006. ICESat over Arctic sea ice: Interpretation of altimetric and reflectivity profiles. *Journal of Geophysical Research*, Vol. 111, C06006, doi:10.1029/2005JC003175.

- Laxon, S., Peacock, N., and Smith, D. 2003. High interannual variability of sea ice thickness in the Arctic region, *Nature*, Vol. 425, pp. 947–949.
- Mätzler, C. 1998. Improved Born approximation for scattering of radiation in a granular medium. *Journal of Applied Physics*, Vol. 83, pp. 6111–6117.
- Mätzler, C. and Wiesmann, A. 1999. Extension of the microwave emission model of layered snowpacks to coarse grained snow. *Remote Sensing of Environment*, Vol. 70, pp. 317–325.
- Mätzler, C., Rosenkranz, P.W., Battaglia, A., and Wigneron, J. P. 2006. *Thermal Microwave Radiation – Applications for Remote Sensing*, IET Electromagnetic Waves Series 52, London, UK.
- McLaren, A. S., Walsh, J. E., Bourke, R. H., Weaver, R. L., and Wittmann, W. 1992. Variability in the sea-ice thickness over the North Pole from 1977 to 1990, *Nature*, Vol. 358, pp. 224–226.
- National Snow and Ice Data Center. 2004. Morphometric characteristics of ice and snow in the Arctic Basin: aircraft landing observations from the Former Soviet Union, 1928–1989. Compiled by Romanov, I. P., Boulder, CO: National Snow and Ice Data Center. Digital media.
- Ridley, J. K. and Partington, K. C. 1988. A model of satellite radar altimeter return from ice sheets. *International Journal of Remote Sensing*, Vol. 9, pp. 601–624.
- Ricker, R., S. Hendricks, J. F. Beckers. The impact of geophysical corrections on sea-ice freeboard retrieved from satellite altimetry. *Remote Sensing* 8, 317, doi:0.3390/rs8040317, 2016.
- Ricker, R., S. Hendricks, V. Helm, H. Skourup, M. Davidson. Sensitivity of CryoSat-2 Arctic sea ice freeboard and thickness on radar-waveform interpretation. *The Cryosphere* 8, 1607-1622, 2014.
- Rothrock, D. A. 1986. Ice thickness distribution – measurement and theory, in: *The Geophysics of Sea Ice*, NATO ASI series B: physics, edited by: Untersteiner, N., Plenum, New York, Vol. 146, pp. 551–575.
- Rothrock, D. A., Zhang, J., and Yu, Y. 2003. The arctic ice thickness anomaly of the 1990s: A consistent view from observations and models, *Journal of Geophysical Research*, Vol. 108, 3083, doi:10.1029/2001JC001208.
- Timco, G. W. and Frederking, R. M. W. 1996. A review of sea ice density. *Cold Regions Science and Technology*, Vol. 24, pp. 1–6.
- Tonboe, R. T., Andersen, S., Gill, R. S., and Toudal Pedersen, L. 2006b. The simulated seasonal variability of the Ku-band radar altimeter effective scattering surface depth in sea ice. *Arctic Sea Ice Thickness: Past, Present and Future*, edited by: Wadhams and Amanatidis, *Climate Change and Natural Hazards Series* 10, EUR 22416.
- Tonboe, R., Andersen, S., and Toudal Pedersen, L. 2006a. Simulation of the Ku-band radar altimeter sea ice effective scattering surface. *IEEE Geoscience and Remote Sensing Letters*, Vol. 3, pp. 237–240.
- Tonboe, R. T., L. T. Pedersen, and C. Haas. 2010. Simulation of the Cryosat-2 satellite radar altimeter sea ice thickness retrieval uncertainty. *Canadian Journal of Remote Sensing*, Vol. 36(1), pp. 55-67.
- Ulaby, F. T., Moore, R. K., and Fung, A. K. 1986. *Microwave Remote Sensing, from Theory to Applications*, vol. 3, pp. 2017-2119. Artech House, Dedham MA.
- Wadhams, P. 1990. Evidence for thinning of the Arctic ice cover north of Greenland, *Nature*, Vol. 345, pp. 795–797.
- Wadhams, P., Tucker III, W. B., Krabill, W. B., Swift, R. N., Comiso, J. C., and Davis, N. R. 1992. Relationship between sea ice freeboard and draft in the Arctic basin and implications for sea ice monitoring, *Journal of Geophysical Research*, Vol. 97, pp. 20325–20334.

- Warren, S. G., Rigor, I. G., Untersteiner, N., Radionov, V. F., Bryazgin, N. N., Aleksandrov, Y. I., and Colony, R. 1999. Snow Depth on Arctic Sea Ice, *Journal of Climate*, Vol. 12, pp. 1814–1829.
- Wingham, D. J., Francis, C. R., Baker, S. 2006. CryoSat: A mission to determine the fluctuations in Earth's land and marine fields, *Advances in Space Research*, Vol. 37, pp. 841–871.
- Wingham, D. 1999. The first of the European Space Agency's opportunity missions: CryoSat, *Earth Observation Quarterly*, Vol. 63, pp. 21–24.

Previous reports

Previous reports from the Danish Meteorological Institute can be found on:
<http://www.dmi.dk/dmi/dmi-publikationer.htm>